Stagnation Temperature and Molecular Weight Effects in Jet Interaction

LARRY J. CHRANS* AND DANIEL J. COLLINS†
Naval Postgraduate School, Monterey, Calif.

The purpose of this study was to investigate the effect of injectant stagnation temperature and molecular weight variation on the flowfield generated from secondary injection of a gas normal to a supersonic stream. Experiments were conducted at a primary stream Mach number of 2.80 in the Naval Postgraduate School supersonic wind tunnel. Experimental data have been correlated with various theories, showing both agreement and disagreement. Data presented include penetration of secondary jet into primary flow and shock shape as correlated with the second-order blast wave theory. Jet momentum, not jet mass, was found to be the main determinant of the observed jet effects.

Nomenclature

A = area
C_D = drag coefficient
C_p = pressure coefficient
c = nozzle discharge coefficient
c_p = specific heat at constant pressure
d = diameter
E = energy, measured per unit length, released in the creation of a shock wave
h = penetration height of secondary fluid into primary stream
Δh = energy transferred from secondary to primary stream
J_o = function of γ_∞ in the blast wave analogy
M = Mach number
$\dot{m}$ = mass flow rate
P = pressure
R = radius of bow wave measured perpendicular to the flat plate axis
$\bar{R}$ = nondimensional blast wave radius
R_j = gas constant of fluid j
R_o = characteristic radius related to the blast wave energy
r = nose radius of equivalent blunt body
T = temperature
t = time
V = velocity
W = molecular weight
x = distance along flat plate axis
$\bar{x}$ = x/R_o
θ = angle between surface of flat plate and injector nozzle axis
γ = specific heat ratio
ρ = density
λ_1 = function of γ_∞ in the blast wave analogy

Superscript

* = pertaining to sonic conditions

Subscripts

j = injectant or secondary fluid
∞ = primary fluid
o = stagnation conditions

Presented as Paper 69-1 at the AIAA 7th Aerospace Sciences Meeting, New York, January 20–22, 1969; received January 15, 1969; revision received August 11, 1969. The authors wish to thank N. Leckenby for his aid in the course of the experiment. The research outlined in this article was supported under a contract from the Navy Air Systems Command, Department of the Navy, Washington, D.C.

* Lieutenant, U.S. Navy.
† Professor, Department of Aeronautics. Associate Fellow AIAA.

Introduction

THE interaction of a lateral jet with a supersonic stream is of fundamental importance to the understanding of complex supersonic flows. The jet interaction application to thrust vector control, reaction control jets, and fuel injection for supersonic combustion is of great engineering interest. Although extensive investigations[1–6] have been conducted of the supersonic gaseous injection phenomena, no systematic investigation of secondary jet stagnation temperature and molecular weight has been made. Most investigations have used sonic injection, so that in the absence of stagnation temperature and molecular weight variations it has not been possible to distinguish between the effects of jet momentum and jet mass addition.

The objective of this investigation was to study the flowfield induced by injecting a gas normal to a supersonic stream, where the primary interest was to discover the effect of injectant stagnation temperature and molecular weight in the flowfield. These studies were performed in the Naval Postgraduate School supersonic wind tunnel at a Mach number of 2.80 by injecting gaseous nitrogen, argon, and helium through a sonic nozzle mounted normal to a flat plate. The parameters varied during the experiments include injectant stagnation pressure and temperature, mass flow rate, molecular weight and injector exit area. By variation of injectant stagnation temperature and molecular weight, distinctions are made between jet mass and jet momentum effects.

Experimental Equipment Report

The injection equipment used in this report was arranged as in Fig. 1. Compressed bottles of gaseous injectant were obtained commercially and fed into the system through a pressure regulator. The flow was then passed through a

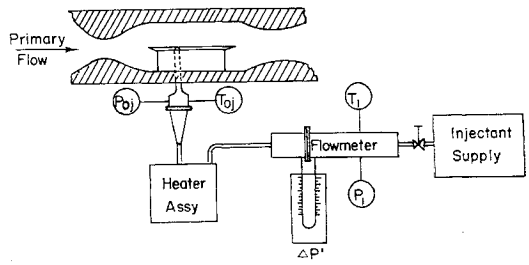

Fig. 1 Injection equipment arrangement.

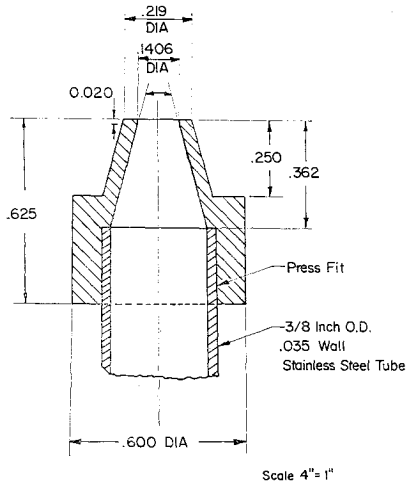

Fig. 2 Sonic nozzle diagram.

flowmeter, into the heater, and on to the sonic nozzle mounted in the flat plate.

The method used to heat the secondary gas was simple, yet effective. Twenty-five ft of $\frac{3}{8}$ in. o.d. stainless steel tube were coiled and placed in an insulated container. Preliminary calculations indicated sonic velocity would be reached inside the heater tube at high temperature and pressure for standard tube diameters smaller than that used. An arc welder was then connected across the ends of the coil, and the coil was heated by passing an electric current through the stainless steel tube. The injectant gas was subsequently heated through contact with the hot tube. The maximum injectant temperature was set at 1800°R due to the structural integrity of the heater at high pressures.

At the heater exit and just prior to the sonic nozzle entrance a device was installed to decrease the velocity of the secondary flow to approximately stagnation conditions. The flow velocity was gently decreased through a 5° diverging section until the cross-sectional area was increased by a factor of ten, ensuring the velocity of the flow through the enlarged section to be less than 0.06 Mach (or approximately stagnation conditions). At this point the temperature and pressure of the secondary fluid were measured, and these values were used in the isentropic equations for a sonic nozzle. A well-rounded converging nozzle was then used to decrease the area ratio prior to entering the sonic nozzle.

The sonic nozzle was a simple converging nozzle with parallel side walls at the exit section. Exit diameters of 0.1406 in. and 0.075 in. were used during the experiments. The sonic nozzle was calibrated by means of an ASME sharp-edged orifice meter. The nozzle discharge coefficient was found to be 0.96. This value is in good agreement with both the theoretical and experimental work of Amick and Hays.[2] The values of the discharge coefficient are estimated to vary from about 0.99 to 0.92. In a series of tests conducted over an order-of-magnitude change in Reynolds number actual variation was less than ±0.03 and in agreement with the theoretical estimates. Figure 2 shows the shape of the nozzle used in the tests. The straight section was approximately 0.020 in. in length. The small straight section was introduced to reduce variations in the value of the nozzle discharge coefficient.

A special phenolic supersonic tunnel block was fabricated to allow the flat plate pedestal to be mounted on the test section floor. The sonic nozzle could then be inserted through the bottom of the test section and through the pedestal without disturbing the flat plate. Thirty-nine static pressure taps were located on the surface of the plate. The generated pressures were measured with a mercury manometer. The side force data will not be discussed in this report.

The NPGS supersonic wind tunnel is a blowdown model with a 4-in. × 4-in. test section, 6 in. long. The tunnel is capable of 5 min of continuous operation at a stagnation pressure of 50 psia. The Reynolds number at the injector port was 8.5×10^6 for $M = 2.8$, ensuring a turbulent boundary layer in the region of the injector nozzle.

The schlieren system used had a standard offset arrangement with collimating mirrors used in place of lenses. The mirrors, light source, and camera were positioned with the aid of a surveyor's transit, so that most of the parallax in the system was eliminated. With this arrangement, shadowgraphs could also be obtained by removing the knife-edge and changing the slit-source to a point source.

Theoretical Analysis

Two properties of the interaction phenomena, penetration height of the secondary fluid and radius of the induced bow shock, will be treated extensively in this article.

The secondary gas is injected into a supersonic stream in the form of a highly underexpanded jet as has been discussed by Schetz and Billig.[3] The secondary jet penetrates the primary stream to a certain height before it is completely bent over and proceeds downstream with the primary fluid. This penetration height depends on the properties of the two streams. Figure 3 illustrates the interaction model of Zukoski and Spaid.[5] Cassel, Davis, and Engh[1] and Hsia[8] have also developed a penetration model. In each of these a penetration height is defined, and the induced shock is noted.

The radius of the induced bow shock can be treated as a function of the penetration height of the secondary fluid[3] or may be calculated from the second-order blast wave analogy, as presented by Broadwell[9] and Dahm.[10]

It is interesting to note that each of the various flow models is based on a blunt-body approximation of the interaction phenomena, but that the results obtained by the model originators varied considerably, due to other basic assumptions made. The primary differences occur due to different selections of a characteristic velocity.

The preceding models were used in this report as a guide for determining which parameters of the flow to vary and then were compared with the experimental results.

Penetration Height

Zukoski and Spaid,[5] in their investigation of injection phenomena, obtained the scaling laws for secondary injection by using an equivalent solid body model. By balancing the drag of the nose section against the momentum flux of the injectant the characteristic dimension of the equivalent solid body is obtained. Since the analysis is readily available in the references only the assumptions and results are presented here. In the Spaid and Zukoski model one has

$$\frac{h}{dc^{1/2}} = \frac{1}{M_\infty}\left(\frac{P_{oj}}{P_\infty}\frac{\gamma_j}{\gamma_\infty}\frac{2}{C_p}\right)^{1/2}\left[\frac{2}{\gamma_j - 1}\left(\frac{2}{\gamma_j + 1}\right)^{\frac{\gamma_j + 1}{\gamma_j - 1}} \times \left(1 - \frac{T_\infty}{T_{oj}}\right)\right]^{1/4} \quad (1)$$

Hsia[8] found in his model the characteristic nose radius was

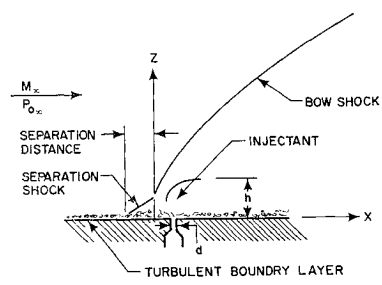

Fig. 3 Zukoski and Spaid flow model.

given by

$$r = [(4/\pi C_D)]^{1/2}(1 + \Delta h/V_\infty{}^2)^{1/2}[(\dot{m}_j/\rho_\infty V_\infty)]^{1/2} \quad (2)$$

Finally Cassel, Davis, and Engh[1] obtained

$$\frac{h}{dc^{1/2}} = \frac{3}{4}\left\{(\gamma_j + 1)\left(\frac{2}{\gamma_j + 1}\right)^{\frac{\gamma_j}{\gamma_j - 1}}\right\}^{1/2} \times \left(\frac{P_{oj}}{q_1}\right)^{1/2} \quad (3)$$

where q_1 is the dynamic pressure.

Although each of the theories discussed here uses a blunt-body model, the use of three different velocities leads to a fundamental difference. Zukoski and Spaid[5] assumed the secondary fluid expanded to the primary stream pressure, P_∞, after leaving the injector nozzle, and therefore the final velocity (V_j) attained was the velocity due to isentropic expansion to that pressure. Hsia[8] assumed the final velocity attained by the secondary fluid was that of the primary stream, V_∞. In the case of Cassel, Davis, and Engh the sonic velocity V^* of the nozzle was taken as the characteristic velocity. This led to a penetration height by Hsia that was jet mass dependent and a penetration height in the case of Zukoski and Spaid and of Cassel, Davis, and Engh, that was jet momentum dependent.

The secondary mass flow from a sonic nozzle is proportional to the stagnation pressure, P_{oj}, and inversely proportional to the square root of stagnation temperature, T_{oj}, of the secondary fluid. The momentum of the secondary fluid leaving the injector nozzle is only proportional to the stagnation pressure of the secondary fluid. The depth of penetration of the secondary fluid into the primary stream will be either jet mass or jet momentum dependent, or a combination of both. Agreement between Zukoski-Spaid[5] and Hsia[8] penetration theory has been previously noted[8] but in the absence of stagnation temperature variation no distinction can be made between the jet mass or the jet momentum effects. The experiments conducted at constant mass flows throws some light on the difference between the characteristic velocities V_j and V^*.

Blast Wave Analogy

The radius of the bow shock caused by secondary injection has been derived in terms of the second-order blast wave equation. Dahm[10] and Broadwell[9] based their theories on the blast wave analogy, where it was assumed that: 1) the secondary fluid is accelerated to the primary stream velocity, V_∞; 2) the energy added per unit length of gas is equal to the change in momentum of the secondary fluid and the heat added to the primary fluid; 3) the blast wave analogy is valid throughout the entire region of the interaction of the primary and the secondary streams in comparison with the penetration height theories.

It can be noted that Zukoski and Spaid[5] also assumed a blunt-nosed body in a hypersonic stream (Newtonian calculations) to find the penetration height of the injectant, but assumed the final velocity the secondary fluid reached was that from expanding to the primary stream pressure, P_∞, instead of the primary stream velocity, V_∞. Thus the blast wave theory is in a sense another equivalent body model.

As Horton and Meade[7] indicate the models of Broadwell[9] and Dahm[10] were based on the blast wave analogy of Hayes.[11] According to Hayes' concept of hypersonic similitude, the pressure, density, and velocity, fields generated by an unyawed, axisymmetric body in a uniform hypersonic flowfield are similar to the pressure, density, and velocity fields generated by the explosion of a line charge. Once the pressure, density, and velocity fields as a function of time t and distance from the line R have been obtained, the corresponding fields for the axisymmetric body are derived by replacing t by x/V_∞, where V_∞ is the velocity of the undisturbed primary flow and x is the distance along the axis of the flat plate from the apex of the detached shock. The concept of similitude is completed by relating the energy released by the line charge to the drag of the body.

Sakurai's[12] second-order solution for the shock wave radius R at any time t in the unsteady problem is given by

$$R = [(2E/\pi J_0 P_\infty)]^{1/4}[1 - \lambda_1[(J_0 P_\infty/2E)]^{1/2} c_\infty t]^{1/2}(c_\infty t)^{1/2} \quad (4)$$

where J_o and λ_1 are constants that depend on the specific heat ratio γ_∞ (for $\gamma_\infty = 1.4$, $J_o = 0.88$ and $\lambda_1 = 1.989$), P_∞ and c_∞ are the pressure and sound speed of the undisturbed primary fluid, and E is the energy, measured per unit length, released in the creation of the shock wave. Assuming $t = x/V_\infty$, Eq. (4) reduces to

$$\bar{R} = \left(\frac{4}{J_o}\right)^{1/4}\left(\frac{\bar{X}}{M_\infty}\right)^{1/2}\left[1 - \lambda_1 \frac{(J_0)^{1/2}}{2}\frac{\bar{X}}{M_\infty}\right]^{1/2} \quad (5)$$

where x is the distance measured from the apex of the bow shock along the centerline of the flat plate, V_∞ is the velocity of the primary fluid at the injectant station,

$$\bar{R} = \frac{R}{R_o}, \bar{X} = \frac{X}{R_o}, \text{ and } R_o = \left(\frac{E}{2\pi P_\infty}\right)^{1/2} \quad (6)$$

is the characteristic radius related to the blast wave energy.

As Broadwell[9] pointed out, E is the energy per unit length in the completely symmetrical case, and for a flat plate all the energy is confined above the plate. Therefore, $E/2$ should be set equal to the total increase in energy due to injection.

As stated in 2) the total energy added per unit length is equal to the change in momentum of the secondary fluid and the heat added to the primary fluid. Broadwell[9] derived the energy term as

$$E = 2\dot{m}_j V_\infty\left[1 + \frac{2 + (\gamma_\infty - 1)M_\infty{}^2}{2(\gamma_\infty - 1)M_\infty{}^2}\frac{W_\infty}{W_j}\frac{T_{oj}}{T_{o\infty}}\right] \quad (7)$$

where the first term represents the energy related to the drag caused by the injectant fluids, and the second term represents the effect of the volume addition by the injectant gas. The development of the energy term by Dahm[10] parallels and extends that of Broadwell[9] but employs significantly different approaches in certain important areas. Dahm derived the energy term for the second-order blast wave radius as

$$E = 2\dot{m}_j V_\infty\left[\frac{1}{2} + \frac{1}{\gamma_\infty(\gamma_\infty - 1)M_\infty{}^2} + \frac{\gamma_j}{\gamma_j - 1}\left(\frac{2 + (\gamma_\infty - 1)M_\infty{}^2}{2\,\gamma_\infty M_\infty{}^2}\frac{W_\infty}{W_j}\frac{T_{oj}}{T_{o\infty}}\right) + \left(\frac{\gamma_j}{\gamma_\infty}\frac{W_\infty}{W_j}\frac{T_{oj}}{T_{o\infty}}\right)^{1/2}\frac{M_j}{M_\infty}\left(\frac{2 + (\gamma_\infty - 1)M_\infty{}^2}{2 + (\gamma_j - 1)M_j}\right)\cos\alpha\right] \quad (8)$$

where α is the angle between the surface of the plate and the axis of the injector ($\cos\alpha = 0$ for normal injection). The terms in the energy equation denote the increase in kinetic energy of the secondary fluid, a mass correction term, the heat added to the primary stream, and the effect of injecting at an angle.

It is interesting to note that although Broadwell developed the energy term, E, from an entirely different viewpoint than that of Dahm, his result agrees very closely for normal injection.

Taking Dahm's value for E, for normal injection Eq. (6) reduces to

$$R_o = \left\{\frac{\dot{m}_j V_\infty}{\pi P_\infty}\left(\frac{1}{2} + \frac{1}{\gamma_\infty(\gamma_\infty - 1)M_\infty{}^2} + \frac{\gamma_j}{\gamma_j - 1}\left[\frac{2 + (\gamma_\infty - 1)M_\infty{}^2}{2\gamma_\infty M_\infty{}^2}\right]\left[\frac{W_\infty}{W_j}\frac{T_{oj}}{T_{o\infty}}\right]\right)\right\}^{1/2} \quad (9)$$

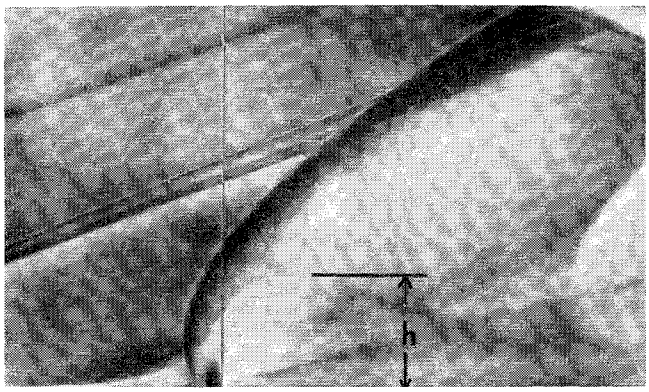

Fig. 4 Schlieren showing penetration height.

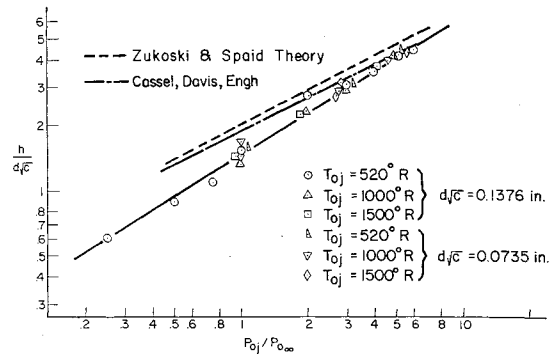

Fig. 6 Penetration height—nitrogen.

Expanding Eq. (9) in terms of the stagnation properties of the primary and secondary streams and assuming a constant primary stream molecular weight, specific heat ratio, and Mach number, then

$$R_o \propto (\dot{m}_j[(T_{o\infty})^{1/2}/P_{o\infty}]\{A + [\gamma_j/(\gamma_j - 1)W_j] \times T_{oj}/T_{o\infty}\})^{1/2} \quad (10)$$

where A is a constant that depends on M_∞. Since

$$\dot{m}_\infty \propto A^* P_{o\infty}/T_{o\infty}{}^{\frac{1}{2}}$$

where A^* is the throat area of the primary nozzle,

$$R_o \propto (\dot{m}_j/\dot{m}_\infty\{A + [\gamma_j/(\gamma_j - 1)W_j]T_{oj}/T_{o\infty}\})^{1/2} \quad (11)$$

Further reduction may be made if for a particular secondary fluid both the primary and secondary flow rates are held constant. Then,

$$R_o \propto [A + BT_{oj}/T_{o\infty}]^{1/2} \quad (12)$$

where $B = B(\gamma_j, W_j)$ and $A = A(M_\infty)$.

Experimental Results

All parameters associated with the primary stream were held constant throughout these experiments. That is, air was used as the primary fluid, and the supersonic tunnel stagnation temperature and pressure and tunnel Mach number were essentially constant for all runs. Therefore, when it is stated that the pressure ratio or mass ratio was varied, in effect, only the injectant pressure or mass was varied. The injectant stagnation pressure was varied from 12.5 to 300 psi, giving a range of pressure ratios from $\frac{1}{4}$ to 6. The injectant stagnation temperature was varied from room temperature (520°R) to 1590°R, giving a range of temperature ratios from 1 to 3. Nitrogen, argon, and helium were used as injectant gases to provide a substantial range for molecular weight effects and also to provide for any heat capacity ratio effects. The sonic nozzle exit diameter was also varied to change the mass flow rate of the injectant while keeping the pressure and temperature constant.

About 80 experimental runs were conducted in an experimental matrix given in Ref. 15. Schlieren photographs were taken of each run, and shadowgraph photographs were taken of many runs. In general the shadowgraph pictures taken did not add to the detail found in the schlieren pictures and, therefore, were not extensively used. The static pressures displayed on the manometer board were also photographed at the same time the schlieren photographs were taken. Polaroid type 55 P/N film was used for each schlieren picture so that the negatives could be enlarged for comparison. The data from the photographs, which included penetration height of the injectant and radius of the bow wave, were obtained by either magnifying the photograph and measuring directly or placing the negative in an optical comparator. A typical photograph is shown in Fig. 4. The penetration height is indicated.

The experimental results are presented in two sections. Figures 5–8 depict the penetration heights obtained by varying each parameter of the secondary flow, and Figs. 9–12 illustrate the variation of the bow shock radius under the same conditions.

Penetration Height

The depth of penetration of the secondary fluid into the primary stream was scaled directly from the photographs and was taken to be the maximum height reached by the bent-over highly underexpanded jet. Figures 5 and 6 show the penetration heights attained by argon and nitrogen; a similar plot not shown was obtained for helium. In each figure the penetration height is plotted as a function of the stagnation pressure ratio, with the runs at various temperatures and nozzle exit diameters included. In each of these figures reference is made to the Zukoski and Spaid[5] theory for penetration height,

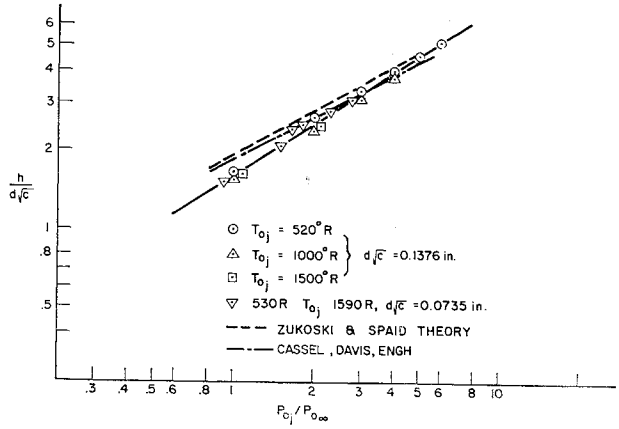

Fig. 5 Penetration height—argon.

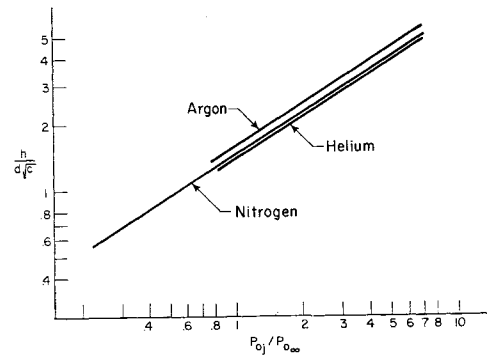

Fig. 7 Composite plot of molecular weight.

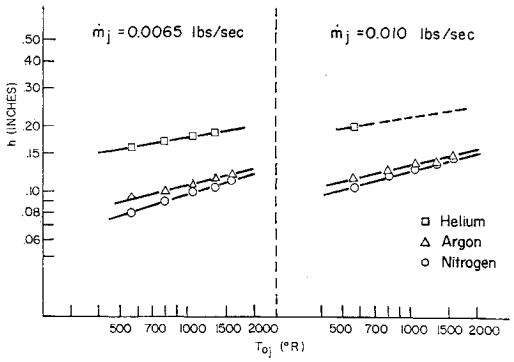

Fig. 8 Penetration height—mass flow rate constant.

and to the Cassel, Davis, and Engh theory, showing agreement with their predictions. Somewhat better agreement is shown for the latter theory. The theory of Schetz and Billig[3] which was developed from Adamson and Nicholls[16] also shows good agreement with the experimental results. Although the stagnation temperature ratio was varied by a factor of three while holding the pressure ratio constant, no essential differences in the penetration height could be detected. Increasing the stagnation temperature of the secondary fluid while holding the pressure constant causes the secondary mass flow rate to decrease. Since the penetration height of the secondary fluid was not affected by this action, the penetration height is either a function of the secondary momentum or at most a weak function of $T_{oj}/T_{o\infty}$. It should be noted that the slope of the line indicating the Zukoski-Spaid theory does not coincide exactly with that plotted from the experimental values obtained.

It was found that for the same quality schlieren photograph the underexpanded helium jet was much more difficult to detect than was the argon or nitrogen jet, so that the corresponding helium plot had fewer experimental points.

Figure 7 is a composite plot of figures for all three gases, showing the mean penetration heights as a function of the stagnation pressure ratio. As indicated there is a difference in the penetration heights of the three gases. The momentum theories are not a function of molecular weight; however, they do provide for gamma variations. Argon and helium, having the same value of heat capacity ratio, should have identical penetration heights under the conditions presented. Nitrogen, having smaller value of heat capacity ratio, should have a penetration height 4% higher than that of argon and helium, as calculated from Eq. (1). This is indeed the case when comparing the penetration heights of nitrogen and helium, but argon lies 10% above nitrogen and 14% above helium. If comparisons with Eq. (3) are made one would expect the nitrogen to lie slightly below the argon and helium. The result may be due to a molecular weight dependence or could possibly be attributed to mixing of the injectant and freestream.

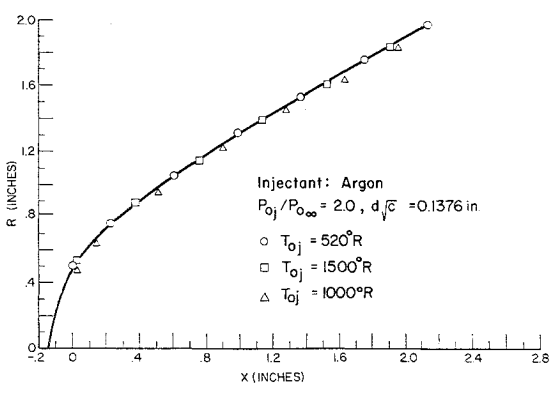

Fig. 9 Shock radius—argon.

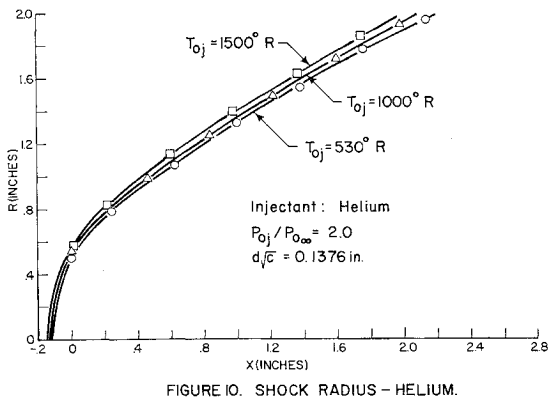

FIGURE IO. SHOCK RADIUS - HELIUM.

Fig. 10 Shock radius—helium.

Equation (1) may be put in the form

$$h \propto [2\gamma_j/(\gamma_j - 1)]^{1/4}(R_jT_{oj})^{1/4}(1/M_\infty)\ (\dot{m}_j/P_\infty)^{1/2} \qquad (13)$$
$$P_\infty/P_{oj} \ll 1$$

Holding the primary stream parameters and the secondary mass flow rate constant, Eq. (13) can be further reduced to

$$h \propto [2\gamma_j/(\gamma_j - 1)]^{1/4}(R_jT_{oj})^{1/4} \qquad (14)$$

A similar equation is obtained using the Cassel, Davis, and Engh theory with a different gamma dependence due to the selection of V^* as the characteristic velocity.

Experiments were next conducted to investigate the penetration height while holding the secondary mass flow rate constant. For each gas considered the stagnation pressure and temperature were adjusted to give a mass flow rate of 0.0065 lbs/sec and 0.010 lbs/sec. The results are presented in Figure 5. It is evident that for a given mass flow rate, the penetration height increases with an increasing stagnation temperature ratio and also increases with a decreasing molecular weight.

If ratios are calculated from the data for the penetration heights for the different gases one finds that the experimental results are in better agreement with the calculated results based upon V^* rather than V_j. This gives further support to the theory of Cassel, Davis, and Engh.

The data shown in Figure 8 scale as the $\frac{1}{2}$ power of $\dot{m}_j$. When the heat capacity ratio dependence was neglected, the data also scaled approximately as the $\frac{1}{4}$ power of the molecular weight, which is in agreement with the theory.

For a given gas (constant molecular weight) and the previously stated conditions,

$$h \propto (T_{oj})^{1/4}$$

There is an expected increase in penetration height of 32% between the temperature of 530°R and 1590°R for all gases. Measured values found from Fig. 6 were 44% increase for argon, 33% for nitrogen, and 20% for helium. The lighter

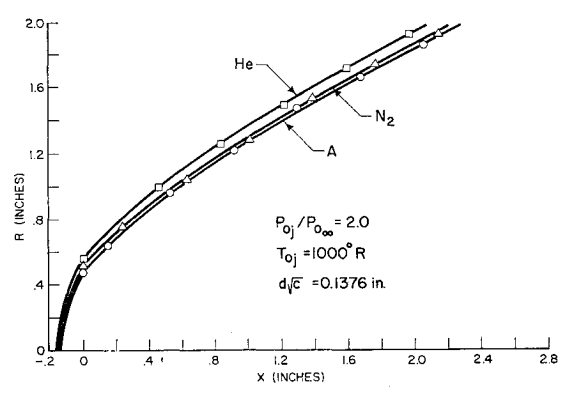

Fig. 11 Shock radius—varying molecular weight.

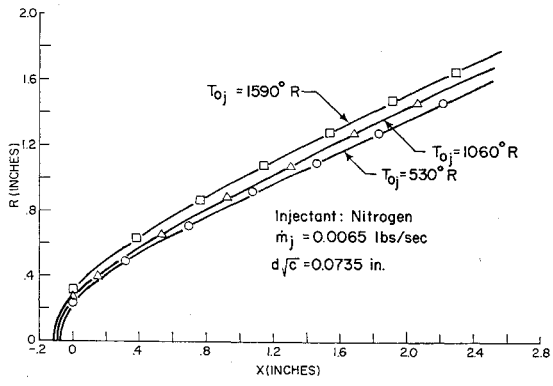

Fig. 12 Shock radius—mass flow constant, varying temperature.

molecular weight gases show less variation with T_{oj} than predicted by theory.

Shock Radius

Figures 9–11 show the shock radius variation for the various gases at a constant pressure ratio, varying temperature. The radius R was measured perpendicular to the flat plate axis at distances x downstream from the injector axis. This presented a fixed reference point from which the actual shock radius could be measured. Comparing these figures, it is apparent that as the molecular weight of the injectant gas decreases, a greater variation occurs in the shock radius with temperature.

Figure 11 shows the variation of the bow shock with molecular weight, while holding the stagnation pressure ratio and temperature ratio constant. Examination of Eqs. (5 and 11) indicates that the radius of the bow shock should vary approximately as $\dot{m}_j^{1/4}[A + BR_j]^{1/8}$ for these conditions, where $A = A(M_\infty)$ and $B = B(\gamma_j, T_{oj})$.

The variation of the bow wave with temperature and molecular weight was very evident in the physical measurement of the radius of the bow wave. When this radius is nondimensionalized with respect to the characteristic radius, R_o, related to the blast wave energy, all radii should converge into a single line if the theory is valid. This is true of the present data using Eq. (5) as shown in Chrans.[15] In each case the measured values followed the pattern set by the second-order theory with what appears to be a constant displacement. However, when the mean lines from the three different molecular weight gases are placed on a composite plot, a molecular weight dependence is present as was the case for the penetration height.

Equation (12) was used as the basis for the next set of experiments, where the injectant mass flow rate was held constant and the radius R was viewed as a function of T_{oj}, W_j, and γ_j. Figure 12 shows the variation of the shock radius

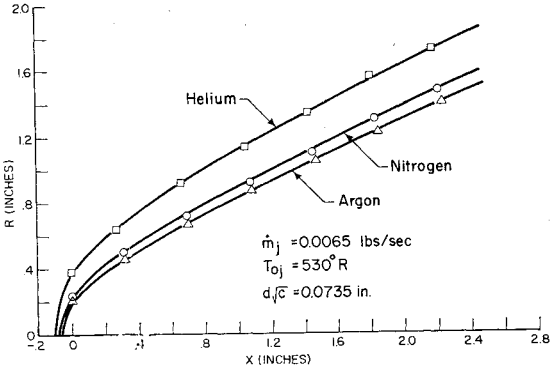

Fig. 13 Shock radius—mass flow constant, varying molecular weight.

Table 1 Variation of shock radius with temperature

Calculated	Measured
$R_{1590}/R_{530} = 1.10$	$R_{1590}/R_{530} = 1.13$
$R_{1060}/R_{530} = 1.06$	$R_{1060}/R_{530} = 1.06$

with injectant stagnation temperature. Equation (12) was used to predict the increase of the radius with temperature. (See Table 1.) Equation (12) was then used to predict the increase of the radius with molecular weight and heat capacity ratio effects, as shown in Fig. 13. The results are shown in Table 2. In general, Eq. (12) showed excellent agreement for the constant secondary mass flow case. In this case the three separate radii collapse into a single line when put in the nondimensional form of Eq. (5).

Conclusions

At constant P_{oj}, varying T_{oj}, the penetration height theory of Cassel, Davis, and Engh[1] showed good agreement with experimental results. The penetration height also showed some dependence on molecular weight, which is contrary to theory. This may be due to mixing. When the secondary mass flow rate was held constant, the penetration height varied with T_{oj}. This rules out any theory based strictly upon a jet mass dependence, as proposed by Hsia[8] in Eq. (2). The penetration height scaled as $(\dot{m}_j)^{1/2}$ as predicted by all theories.

Ignoring heat capacity ratio effects, that is the gamma dependence, the penetration height scaled roughly as $(R_j)^{1/4}$ which is in agreement with the jet momentum theory of Zukoski and Spaid. Assuming a different characteristic velocity of the secondary flow (using V^* instead of V_j), good agreement was obtained with theory without having to ignore the heat capacity ratio effects. This is in agreement with Cassel, Davis, and Engh.

In general, the penetration height, as a function of T_{oj}, differed for different molecular weights. When penetration height was considered as a function of P_{oj}, the experimental results for the penetration height showed good agreement with the momentum theories for both the constant P_{oj} and constant mass flow runs. The penetration height is either not a function of T_{oj} or is, at most, a weak function of T_{oj}.

The radius of the blast wave measured from the experimental data was in close agreement with that predicted by Dahm. The blast wave theory was not able to predict the molecular weight variation accurately when the pressure and temperature of the system were varied but showed good agreement when the secondary mass flow was held constant.

The penetration height, h, was found to remain constant for varying temperature, whereas the bow shock radius R varied with temperature. An attempt was made to nondimensionalize the height of penetration with respect to the characteristic blast wave radius, R_o. Figure 14 indicates that as $T_{oj}/T_{o\infty}$ increases at constant mass flow, there is a divergence with respect to molecular weight of h/R_o. This is because h does not vary as T_{oj} increases whereas R_o does vary as a function of temperature and molecular weight. Typical values are: argon

$$R_o \propto [0.728 + 0.427\ T_{oj}/T_{o\infty}]^{1/2}$$

Table 2 Variation of shock radius with molecular weight

Calculated	Measured
$R_{He}/R_A = 1.23$	$R_{He}/R_A = 1.29$
$R_{N_2}/R_A = 1.04$	$R_{N_2}/R_A = 1.06$
$R_{He}/R_{N2} = 1.17$	$R_{He}/R_{N2} = 1.22$

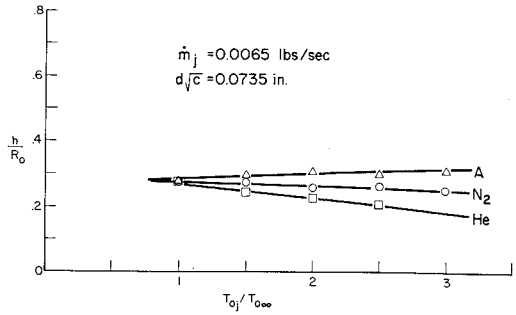

Fig. 14 Comparison of characteristic dimensions—mass flow constant.

nitrogen

$$R_o \propto [0.728 + 0.848\ T_{oj}/T_{0\infty}]^{1/2}$$

helium

$$R_o \propto [0.728 + 4.28\ T_{oj}/T_{o\infty}]^{1/2}$$

In general, the comparisons between the characteristic dimensions, h and R_o, and the experimental data indicate that h would be a good engineering correlation parameter for secondary nitrogen and argon flows but would be less accurate for the lighter molecular weight gases such as helium.

Since the side force is proportional to the interaction area, the data would support the contention that if the stagnation pressure is held constant, there is no appreciable effect of heating on side force. The beneficial effect of heating, or of using a light gas, is the reduction of the mass flow for a given stagnation pressure.

References

[1] Cassel, L. A., Davis, J. G., and Engh, D. P., "Lateral Jet Control Effectiveness Prediction for Axisymmetric Missile Configurations," Rept. RD-TR-68-5, U.S. Army Missile Command, Redstone Arsenal, June 1968.

[2] Amick, J. L. and Hays, P. B., "Interaction Effects of Side Jets Issuing From Flat Plates and Cylinders Alined with a Supersonic Stream," TR 60-329, June 1960, Wright Air Development Division.

[3] Schetz, J. A. and Billig, F. S., "Penetration of Jets into a Supersonic Stream," *Journal of Spacecraft and Rockets*, Vol. 3, No. 11, Nov. 1966, pp. 1658–1665.

[4] Hawk, N. W. and Amick, J. L., "Two-Dimensional Secondary Interaction with a Supersonic Stream," *AIAA Journal*, Vol. 5, No. 4, April 1967, pp. 655–660.

[5] Zukoski, E. E. and Spaid, F. W., "Secondary Injection of Cases into a Supersonic Flow," *AIAA Journal*, Vol. 2, No. 10, Oct. 1964, pp. 1689–1696.

[6] Walker, R. E., Stone, A. R., and Shandor, M., "Secondary Gas Injection in a Conical Rocket Nozzle," *AIAA Journal*, Vol. 1, No. 2, Feb. 1963, pp. 334–338.

[7] Horton, T. R. and Meade, A. J., "Thrust Vector Control of Rocket Engines by Gaseous Injection: A Critical Appraisal of Theoretical Models," TR 67/7, Rocket Propulsion Establishment, Wescott, England, 1967.

[8] Hsia, H. T. S., "Equivalence of Secondary Injection to a Blunt Body in Supersonic Flow," *AIAA Journal*, Vol. 4, No. 10, Oct. 1966, pp. 1832–1834.

[9] Broadwell, J. E., "Analysis of the Fluid Mechanics of Secondary Injection for Thrust Vector Control," *AIAA Journal*, Vol. 1, No. 5, May 1963, pp. 1067–1075.

[10] Dahm, T. J., "The Development of an Analogy to Blast-Wave Theory for the Prediction of Interaction Forces Associated with Gaseous Secondary Injection into a Supersonic Stream," VIDYA TN 9166-TN-3, May 1964, Vidya Division of Itek Corporations.

[11] Hayes, W. D., "On Hypersonic Similitude," *Quarterly Journal of Applied Mathematics*, Vol. 5, No. 105, 1947.

[12] Sakurai, A., "On the Propagation and Structure of a Blast Wave," *Journal of the Physical Society of Japan*, Pt. I, Vol. 8, 1953, pp. 652–659; Part II, Vol. 9, 1954, pp. 256–266.

[13] Stearns, R. F. et al., *Flow Measurement with Orifice Meters*, Van Nostrand, New York, 1951.

[14] Shapiro, A. H., *The Dynamics and Thermodynamics of Compressible Fluid Flow*, Vols. 1 and 2, Ronald Press, New York, 1953.

[15] Chrans, L. F., "The Effect of Stagnation Temperature and Molecular Weight Variation of Gaseous Injection into a Supersonic Stream," thesis, Sept. 1968, Naval Postgraduate School.

[16] Adamson, T. C. and Nicholls, J. A., "On the Structure of Jets from Highly Underexpanded Nozzles into Still Air," *Journal of the Aerospace Sciences*, Vol. 26, No. 1, Jan. 1959, pp. 16–24.